Thermoelectrics in Coulomb-coupled quantum dots: Cotunneling and energy-dependent lead couplings

Nicklas Walldorf,* Antti-Pekka Jauho, and Kristen Kaasbjerg†
Center for Nanostructured Graphene (CNG), Department of Micro- and Nanotechnology, Technical University of Denmark, DK-2800 Kongens Lyngby, Denmark
(Received 1 June 2017; published 8 September 2017)

We study thermoelectric effects in Coulomb-coupled quantum-dot (CCQD) systems beyond lowest-order tunneling processes and the often applied wide-band approximation. To this end, we present a master-equation (ME) approach based on a perturbative T-matrix calculation of the charge and heat tunneling rates and transport currents. Applying the method to transport through a noninteracting single-level QD, we demonstrate excellent agreement with the Landauer-Büttiker theory when higher-order (cotunneling) processes are included in the ME. Next, we study the effect of cotunneling and energy-dependent lead couplings on the heat currents in a system of two CCQDs. We find that cotunneling processes (i) can dominate the off-resonant heat currents at low temperature and bias compared to the interdot interaction, and (ii) give rise to a pronounced reduction of the cooling power achievable with the recently demonstrated Maxwell's demon cooling mechanism. Furthermore, we demonstrate that the cooling power can be boosted significantly by carefully engineering the energy dependence of the lead couplings to filter out undesired transport processes. Our findings emphasize the importance of higher-order cotunneling processes as well as engineered energy-dependent lead couplings in the optimization of the thermoelectric performance of CCQD systems.

DOI: 10.1103/PhysRevB.96.115415

I. INTRODUCTION

The experimental progress in the control of single-electron transport [1] has spurred interest in nanosystems that utilize the associated heat currents for thermoelectric applications [2–4]. In particular, experiments with Coulomb-coupled quantum-dot (CCQD) systems have demonstrated a plethora of phenomena ranging from Coulomb drag [5,6] and electron pairing [7] to extraordinary thermoelectric effects [8,9]. This includes the realization of an energy harvester that converts a thermal gradient in a CCQD system into an electric current [8], as well as an autonomous Maxwell's demon capable of cooling a current-carrying QD system at the cost of heating a "demon" QD system [9].

In addition to the above, theoretical studies have predicted a wide range of novel thermoelectric effects in CCQD systems [10–13]. The mechanisms behind these effects rely on the presence of a strong Coulomb interaction between electrons in the otherwise decoupled QDs (see Fig. 1 for the case of two Coulomb-coupled QDs). The strong interaction can be utilized to tailor the thermoelectric properties of CCQD systems [4,14], and it provides the opportunity to test fundamental thermodynamic aspects of heat transport in interacting nanoscale systems driven out of equilibrium [15].

While the operation principles of the above-mentioned effects are governed by *incoherent* electron tunneling (sequential tunneling) processes between the leads and the QDs [8–13], the importance of coherent higher-order tunneling (cotunneling) processes for nonlinear heat transport remains largely unexplored. Furthermore, when operated under strong nonequilibrium conditions in which linear-response theory breaks down, a theoretical treatment taking into account the full nonlinear properties is needed [16–19]. Only recently have these issues been discussed in strongly interacting QD systems [9,20–22].

Another important factor for thermoelectric effects in CCQD systems is the coupling to the leads, which is usually treated in the wide-band approximation assuming energy-independent couplings [23]. However, energy-dependent couplings to the leads occur naturally in many QD systems [5,6,8,24] and add an important degree of tunability to the system. This is as crucial for the thermoelectric properties [10,11,25] as it is for Coulomb drag [5,6,26–28].

In this work, we present a master-equation approach for the calculation of the nonlinear electronic charge and heat currents in interacting QD systems that takes into account the above-mentioned factors. The charge and heat transfer rates produced by electron tunneling processes are obtained with a perturbative T-matrix approach [23], which treats sequential and cotunneling processes on an equal footing. We resolve the technical challenges associated with the evaluation of the cotunneling rates with an implementation of the often applied regularization scheme [29,30], which applies to the general case of energy-dependent lead couplings, applied biases, and temperature gradients in the system.

The main findings and the organization of the paper are as follows. In Sec. II we introduce the model system of CCQDs. In Sec. III we present the methodology, and we benchmark the approach in Sec. IV by comparing it to the Landauer-Büttiker result for transport through a noninteracting single-level QD. In Sec. V we study nonlinear thermoelectric phenomena in CCQDs. We investigate the energy exchange mediated by the interdot Coulomb interaction, which among other thermoelectric effects leads to the demon-induced cooling mechanism [9,10]. Our findings shed light on the limitations imposed by cotunneling processes on the performance of this mechanism. Furthermore, we demonstrate a strongly enhanced performance of the demon-induced cooling effect by tuning the

*nicwall@nanotech.dtu.dk
†kkaa@nanotech.dtu.dk

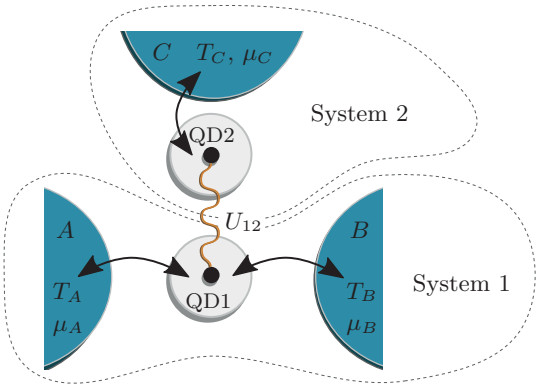

FIG. 1. Illustration of the CCQD system studied in Sec. V consisting of two Coulomb-coupled QDs with interdot Coulomb interaction U_{12} (no tunneling is allowed between the QDs) in a three-terminal configuration with leads $\ell \in \{A, B, C\}$ with temperatures T_ℓ and electrochemical potentials μ_ℓ.

energy dependence of the lead couplings. In such performance optimization, as we show, cotunneling processes are essential for a quantitative description of the thermoelectric properties. Finally, Sec. VI presents our conclusions, and the appendix provides technical details on the cotunneling rates and the regularization procedure.

II. COULOMB-COUPLED QD SYSTEMS

We consider CCQD systems like the one illustrated in Fig. 1, which can be described by the Hamiltonian

$$\hat{H} = \hat{H}_{\text{dots}} + \hat{H}_{\text{leads}} + \hat{H}_T, \tag{1}$$

and consists of a system of CCQDs with Hamiltonian $\hat{H}_{\text{dots}}$ that is coupled to external leads with Hamiltonian $\hat{H}_{\text{leads}}$ by tunnel couplings described by $\hat{H}_T$. We denote $\hat{H}_0 = \hat{H}_{\text{dots}} + \hat{H}_{\text{leads}}$.

We consider a spinless model of Coulomb-coupled single-level QDs described by the Hamiltonian

$$\hat{H}_{\text{dots}} = \sum_\delta \epsilon_\delta \hat{c}_\delta^\dagger \hat{c}_\delta + \sum_{\langle \delta, \delta' \rangle} U_{\delta\delta'} \hat{n}_\delta \hat{n}_{\delta'}, \tag{2}$$

where $\hat{c}_\delta^\dagger$ ($\hat{c}_\delta$) creates (annihilates) an electron in QD δ with energy controlled by gate voltages $\epsilon_\delta = -eV_\delta$, where V_δ is the gate potential on dot δ, $\hat{n}_\delta = \hat{c}_\delta^\dagger \hat{c}_\delta$ is the occupation number operator, $U_{\delta\delta'}$ is the interdot Coulomb interaction, and the summation in the second term is over all QD pairs (specific systems are studied in Secs. IV–V). Intradot double occupancy can be neglected due to a large intradot Coulomb interaction.

The leads are described by noninteracting electron reservoirs, $\hat{H}_{\text{leads}} = \sum_{\ell k} \epsilon_{\ell k} \hat{c}_{\ell k}^\dagger \hat{c}_{\ell k}$, where $\hat{c}_{\ell k}^\dagger$ ($\hat{c}_{\ell k}$) creates (annihilates) an electron with momentum k and energy $\epsilon_{\ell k}$ in lead ℓ, which is assumed to be in local equilibrium with temperature T_ℓ and electrochemical potential $\mu_\ell = \mu_0 - eV_\ell$, where μ_0 is the equilibrium chemical potential and V_ℓ is the voltage applied to lead ℓ. The tunneling Hamiltonian that couples the QD system to the leads is $\hat{H}_T = \sum_{\ell k \delta} (t_{\ell k \delta} \hat{c}_\delta^\dagger \hat{c}_{\ell k} + \text{H.c.})$, where $t_{\ell k \delta}$ is the tunneling amplitude. We define lead coupling strengths as $\gamma^\ell(\epsilon) \equiv 2\pi d_\ell(\epsilon) |t_\ell(\epsilon)|^2$, where $d_\ell(\epsilon)$ is the lead density of states. $\gamma^\ell(\epsilon)$ is allowed to be energy-dependent in contrast to the often applied wide-band approximation.

III. MASTER EQUATION AND TRANSPORT CURRENTS

We describe the dynamics and transport in the CCQD system with a Pauli ME, where the transitions between the QD states are governed by electron tunneling to and from the leads [31]. The tunneling-induced transition rates are calculated based on a perturbative T-matrix approach in which the tunneling Hamiltonian is treated as a perturbation to the decoupled QD system and leads. This allows for a systematic expansion in the tunnel couplings and the inclusion of high-order processes. However, quantum effects such as tunneling-induced level broadening and level shifts [32–34] are not captured by this perturbative approach, which is only valid in the weak-coupling regime $\gamma < k_B T, U$.

In the absence of tunnel coupling, the states of the decoupled QD system and leads are described by product states of the QD system occupation states $|m\rangle$ with energy $E_{\text{dots},m} = \langle m|\hat{H}_{\text{dots}}|m\rangle$ and the leads $|i\rangle$ with energy $E_{\text{leads},i} = \langle i|\hat{H}_{\text{leads}}|i\rangle$. The nonequilibrium occupations of the QD states are described by probabilities p_m (the diagonal components of the reduced density operator of the CCQD system), which are determined by the ME,

$$\dot{p}_m = \sum_{n \neq m} (\Gamma_{nm} p_n - \Gamma_{mn} p_m), \quad \sum_m p_m = 1, \tag{3}$$

where Γ_{mn} denotes the tunneling-induced transition rate from QD state $|m\rangle$ to $|n\rangle$. The ME is solved for the steady-state probabilities, $\dot{p}_m = 0$, in the following. The QD states are given explicitly in Secs. IV and V for the considered systems.

A. Transition rates

The rates for transitions between the QD states are obtained from the generalized Fermi's golden rule [23,35]

$$\tilde{\Gamma}_{mn} = \frac{2\pi}{\hbar} \sum_{ij} |\langle j|\langle n|T|m\rangle|i\rangle|^2 \rho_i \times \delta(\Delta_{mn} + E_{\text{leads},j} - E_{\text{leads},i}), \tag{4}$$

where $\Delta_{mn} \equiv E_{\text{dots},n} - E_{\text{dots},m}$, ρ_i is the thermal probability of finding the leads in the initial state, the sum is over initial and final states of the leads, and the T matrix obeys

$$\hat{T} = \hat{H}_T + \hat{H}_T \frac{1}{E_{\text{initial}} - \hat{H}_0 + i\eta} \hat{T}, \tag{5}$$

with $E_{\text{initial}} = E_{\text{dots},m} + E_{\text{leads},i}$, and η is a positive infinitesimal.

The lowest-order contribution to the tunneling rates describes single-electron tunneling, or *sequential tunneling*, processes between the QD system and the leads:

$$\Gamma_{mn}^{\overrightarrow{\ell}} = \hbar^{-1} \gamma^\ell(\Delta_{mn}) f^\ell(\Delta_{mn}), \tag{6}$$

$$\Gamma_{mn}^{\overleftarrow{\ell}} = \hbar^{-1} \gamma^\ell(\Delta_{nm}) \bar{f}^\ell(\Delta_{nm}), \tag{7}$$

where Eq. (6) [Eq. (7)] is the sequential rate of tunneling out of, $\rightarrow$, (into, $\leftarrow$,) lead ℓ, thereby changing the state of the

QD system from m to n, $f^{\ell}(\epsilon) = \{\exp[\beta_\ell(\epsilon - \mu_\ell)] + 1\}^{-1}$ is the Fermi-Dirac distribution in lead ℓ, $\bar{f}^{\ell}(\epsilon) = 1 - f^{\ell}(\epsilon)$, and $\beta_\ell = 1/(k_B T_\ell)$. The leads are assumed to equilibrate to the Fermi-Dirac distribution in between the tunneling events.

The next-to-leading order terms in the T matrix describe cotunneling processes. In conventional *local* elastic and inelastic cotunneling processes, a net electron is transferred between two leads attached to the same QD (e.g., System 1 in Fig. 1). Here we also consider (i) *nonlocal* cotunneling processes [27,36] in which a net electron is transferred between leads attached to different QDs, as well as (ii) pair-cotunneling processes in which two electrons tunnel into/out of the CCQD system in one coherent process [37,38].

For the thermoelectric effects in focus here, the process of nonlocal cotunneling is important. The (unregularized) rate for nonlocal cotunneling that net transfers an electron out of lead ℓ and into lead ℓ' is given by

$$\tilde{\Gamma}^{\overrightarrow{\ell}\,\overleftarrow{\ell'}}_{mn} = \int \frac{d\epsilon}{2\pi\hbar}\gamma^{\ell}(\epsilon)\gamma^{\ell'}(\epsilon - \Delta_{mn}) f^{\ell}(\epsilon)\bar{f}^{\ell'}(\epsilon - \Delta_{mn}) \times \left|\frac{1}{\Delta_{vm} + \epsilon + i\eta} + \frac{1}{\Delta_{v'n} - \epsilon + i\eta}\right|^2, \tag{8}$$

where v (v') refers to the virtually occupied intermediate state in the process in which an electron initially tunnels from lead ℓ and into the QD system (from the QD system and into lead ℓ'). We refer the reader to the appendix for the expressions for the remaining cotunneling processes relevant for this study.

A well-known artifact of the cotunneling rates obtained with the T-matrix approach is that they formally diverge in the limit $\eta \to 0$. To deal with this divergence, different regularization schemes have been proposed [29,30,35,39]. Deep inside the Coulomb blockade, the discrepancy between the different regularization schemes vanishes [39]. In this work, we apply the by now standard regularization scheme in Ref. [29], but for future work a detailed comparison of the heat currents obtained from different regularization schemes could be useful. We denote the regularized rates that enter into Eq. (3) without a tilde. To be explicit, we consider the processes $\Gamma_{mn} \equiv \sum_\ell(\Gamma^{\ell\leftarrow}_{mn} + \Gamma^{\ell\rightarrow}_{mn})$, $\Gamma^{\ell\leftarrow}_{mn} \equiv \Gamma^{\overleftarrow{\ell}}_{mn} + \sum_{\ell'}(\Gamma^{\overleftarrow{\ell}\,\overrightarrow{\ell'}}_{mn} + \Gamma^{\overleftarrow{\ell}\,\overleftarrow{\ell'}}_{mn})$, $\Gamma^{\ell\rightarrow}_{mn} \equiv \Gamma^{\overrightarrow{\ell}}_{mn} + \sum_{\ell'}(\Gamma^{\overrightarrow{\ell}\,\overleftarrow{\ell'}}_{mn} + \Gamma^{\overrightarrow{\ell}\,\overrightarrow{\ell'}}_{mn})$. A numerical procedure for the regularization is outlined in the appendix.

B. Charge and heat currents

The steady-state transport currents can be obtained from the occupation probabilities. The electric current going into lead ℓ is

$$I_\ell \equiv -e\left\langle \sum_k \frac{d\hat{n}_{\ell k}}{dt}\right\rangle = -e\sum_{mn} p_m\left(\Gamma^{\ell\leftarrow}_{mn} - \Gamma^{\ell\rightarrow}_{mn}\right), \tag{9}$$

where $\hat{n}_{\ell k} = \hat{c}^\dagger_{\ell k}\hat{c}_{\ell k}$, p_m is calculated from the steady-state solution of Eq. (3), and the rightmost form expresses the electric current in terms of the total rate of electrons tunneling into lead ℓ minus the total rate of electrons tunneling out of lead ℓ [40].

The heat current going into lead ℓ is [15,17,41]

$$J_\ell \equiv \left\langle \sum_k (\epsilon_{\ell k} - \mu_\ell)\frac{d\hat{n}_{\ell k}}{dt}\right\rangle = \sum_{mn} p_m\left(W^{\ell\leftarrow}_{mn} - W^{\ell\rightarrow}_{mn}\right), \tag{10}$$

where the rightmost form expresses the heat current in terms of heat rates W (using a similar notation to that for the tunneling rates).

The sequential-tunneling heat rate in lead ℓ is calculated as the tunneling rate multiplied by the energy of the tunneling electron relative to the chemical potential in the lead,

$$W^{\overrightarrow{\ell}}_{\ell,mn} = (\Delta_{mn} - \mu_\ell)\Gamma^{\overrightarrow{\ell}}_{mn}, \quad W^{\overleftarrow{\ell}}_{\ell,mn} = (\Delta_{nm} - \mu_\ell)\Gamma^{\overleftarrow{\ell}}_{mn}, \tag{11}$$

where the indices follow the notation of the tunneling rates, and the additional subscript ℓ refers to the lead in which the heat rate is calculated.

Analogously, the cotunneling heat rates into/out of the leads are calculated *a posteriori* by multiplying the integrand in the cotunneling rate by the energy of the tunneling electron relative to the chemical potential of the lead. For example, for the nonlocal cotunneling process between lead ℓ and ℓ', the (unregularized) heat rate in lead ℓ reads

$$\tilde{W}^{\overrightarrow{\ell}\,\overleftarrow{\ell'}}_{\ell,mn} = \int \frac{d\epsilon}{2\pi\hbar}\gamma^{\ell}(\epsilon)\gamma^{\ell'}(\epsilon - \Delta_{mn}) f^{\ell}(\epsilon)\bar{f}^{\ell'}(\epsilon - \Delta_{mn}) \times (\epsilon - \mu_\ell)\left|\frac{1}{\Delta_{vm} + \epsilon + i\eta} + \frac{1}{\Delta_{v'n} - \epsilon + i\eta}\right|^2, \tag{12}$$

with the heat rate in lead ℓ', $\tilde{W}^{\overrightarrow{\ell}\,\overleftarrow{\ell'}}_{\ell',mn}$, given as above but with $(\epsilon - \mu_\ell)$ replaced by $(\epsilon - \Delta_{mn} - \mu_{\ell'})$. The remaining cotunneling heat rates follow similarly.

Whereas the calculation of charge currents involves the electron-tunneling rates that enter the ME (3), and therefore does not require any additional steps once the ME has been set up and solved, the heat currents must be calculated via the heat tunneling rates in a postprocessing step, similar to the procedure in full density-matrix treatments [20].

IV. COMPARISON TO THE LANDAUER-BÜTTIKER FORMALISM

In this section, we benchmark the approach by comparing the charge and heat currents in a spinless noninteracting single-level QD system with those obtained from the Landauer-Büttiker (LB) formalism (see Ref. [42] for a comparison of the electric current in the case of equal temperatures in the leads). For noninteracting systems, the LB result is exact. However, for the thermoelectric effects discussed in Sec. V, which require the presence of strong Coulomb interaction, an alternative method such as the ME approach is needed.

We consider a single-level QD coupled to two leads $\ell \in \{A, B\}$ (such as System 1 in Fig. 1 when decoupled from System 2). For simplicity, we assume wideband lead couplings $\gamma^{\ell}(\epsilon) = \gamma^{\ell}$ in this case. The Hamiltonian of the QD reduces to

$$\hat{H}_{\rm dots} = \epsilon_1\hat{c}^\dagger_1\hat{c}_1, \tag{13}$$

with states labeled by the occupancy, $|n_1\rangle \in \{|0\rangle, |1\rangle\}$.

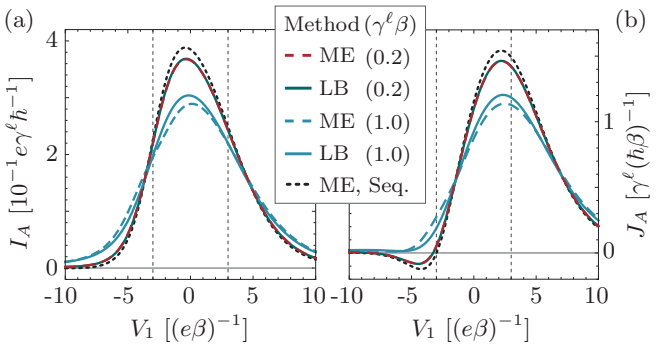

FIG. 2. Comparison of the electric current (a) and heat current (b) calculated with the ME and LB approaches. Currents are plotted as a function of gate voltage V_1 for two different lead coupling strengths $\gamma^A = \gamma^B = \gamma^\ell$ (energy-independent). The ME result including only sequential tunneling is shown for reference (black dotted), and the vertical dashed lines mark the alignment of the dot level with the electrochemical potentials of leads A (left) and B (right). Parameters: $T_B = 2T_A \equiv 2/(k_B\beta)$, $\mu_A = 3\,\beta^{-1}$, $\mu_B = -3\,\beta^{-1}$, and $\eta = 10^{-3}\,\beta^{-1}$.

In the LB formalism, the electric current and heat current going into lead A are given by [18,43]

$$I_A^{\mathrm{LB}} = \frac{-e}{h}\int d\epsilon\, T(\epsilon)[f^B(\epsilon) - f^A(\epsilon)] \tag{14}$$

and

$$J_A^{\mathrm{LB}} = \frac{1}{h}\int d\epsilon\,(\epsilon - \mu_A)T(\epsilon)[f^B(\epsilon) - f^A(\epsilon)], \tag{15}$$

respectively. For a noninteracting single-level QD, the transmission function $T(\epsilon)$ is

$$T(\epsilon) = \frac{\gamma^A\gamma^B}{(\epsilon-\epsilon_1)^2 + (\gamma/2)^2}, \tag{16}$$

where $\gamma = \gamma^A + \gamma^B$ and we have omitted the tunneling-induced energy shift, which is not captured by the T-matrix approach.

The transport currents calculated with the two approaches with a finite bias and temperature difference ($T_B = 2T_A \equiv 2T$) between the leads are plotted in Figs. 2(a) and 2(b) as a function of the gate voltage for two different lead coupling strengths. To demonstrate the importance of cotunneling processes, we have included ME results based on sequential tunneling only (black dotted curves) that do not depend on γ^ℓ in the units shown, as well as sequential plus cotunneling (dashed curves). The results based purely on sequential tunneling differ significantly from the LB results unless $\gamma^\ell \ll k_BT$. However, for $\gamma^\ell < k_BT$, the ME results with cotunneling are in excellent agreement with the LB formalism. For $\gamma^\ell > k_BT$, which is outside the regime of validity of the ME approach, the two approaches deviate as expected.

In the following discussion of thermoelectric effects, the heat current is of particular interest. As seen in Fig. 2(b), when the dot level is above the electrochemical potential in lead A, the heat current becomes negative (for sufficiently small lead coupling strength). In this case, electrons above the electrochemical potential tunnel out of the lead and thereby cool the lead [cf. Eq. (10)]. Such cooling mechanisms due to energy-selective tunneling have been confirmed experimentally in metallic QD systems [9,44]. The energy-selective tunneling gives rise to an asymmetry in the energy dissipation between the source and drain leads that was recently observed in molecular junctions [45].

V. THERMOELECTRIC EFFECTS IN COULOMB-COUPLED QDs

In the remaining part of the paper, we study the thermoelectric properties of the system illustrated in Fig. 1, i.e., two single-level QDs with QD1 tunnel-coupled to leads A and B and QD2 tunnel-coupled to lead C. The CCQD system is described by the Hamiltonian

$$\hat{H}_{\mathrm{dots}} = \epsilon_1\hat{c}_1^\dagger\hat{c}_1 + \epsilon_2\hat{c}_2^\dagger\hat{c}_2 + U\hat{n}_1\hat{n}_2, \tag{17}$$

where we have used the simplified notation $U_{12} \equiv U$, and the occupation states are $|m\rangle = |n_1n_2\rangle \in \{|00\rangle,|10\rangle,|01\rangle,|11\rangle\}$. We consider situations in which a source-drain bias V is applied to System 1, $\mu_A = \mu_0 + eV/2$, $\mu_B = \mu_0 - eV/2$ (we set $\mu_0 = 0$ for reference).

As pointed out above, we allow here for energy-dependent lead couplings. For small bias voltages and temperature differences compared to the energy scale at which the lead couplings vary, it suffices to consider the expansion of the lead couplings around their value at μ_0 [46],

$$\gamma^\ell(\epsilon) = \gamma_0^\ell + (\epsilon - \mu_0)\partial\gamma^\ell, \tag{18}$$

where $\gamma_0^\ell = \gamma^\ell(\mu_0)$, $\partial\gamma^\ell \equiv \frac{\partial\gamma^\ell(\epsilon)}{\partial\epsilon}|_{\epsilon=\mu_0}$.

A. Current and energy exchange

In Fig. 3(a) we show the electric current through QD1, $I \equiv I_A = -I_B$, at low temperature $k_BT_\ell = 10^{-2}U$ (for illustrative convenience) and bias $eV = 0.3U$ as a function of gate detuning $V_2 - V_1$ and total gating $V_1 + V_2$ in the vicinity of the honeycomb vertex of the stability diagram [47]. Here, we initially assume energy-independent lead couplings, which is sufficient to get an overall understanding of the behavior of the system. The large current near the degeneracy lines defined by $\Delta_{00,10} = 0$ and $\Delta_{01,11} = 0$ is due to sequential tunneling processes. Away from these degeneracy lines where sequential tunneling is exponentially suppressed, cotunneling processes give rise to a weak background current. At the degeneracy line $\Delta_{10,01} = 0$ connecting the two triple points at $(V_1,V_2) = (0,0),(U,U)$, respectively, *nonlocal* cotunneling processes are responsible for the enhanced cotunneling current [27].

The heat currents that accompany the electric current are shown in Figs. 3(b)–3(d) for different temperatures in the leads. Figure 3(b) shows the heat current in lead A for $k_BT_\ell = 0.1U$. Near the degeneracy lines where $\Delta_{00,10} = 0$ and $\Delta_{01,11} = 0$ and only the occupation of QD1 fluctuates, the heat current shows a behavior similar to that in Fig. 2(b) for a single-level QD. However, at the center of the stability diagram, Coulomb-mediated energy exchange due to the strong Coulomb interaction between the QDs becomes significant. This manifests itself in a cooling of System 1 inside the region bounded by the solid lines at the center of Fig. 3(b) (notice that the color scale is dominated by the heat current with

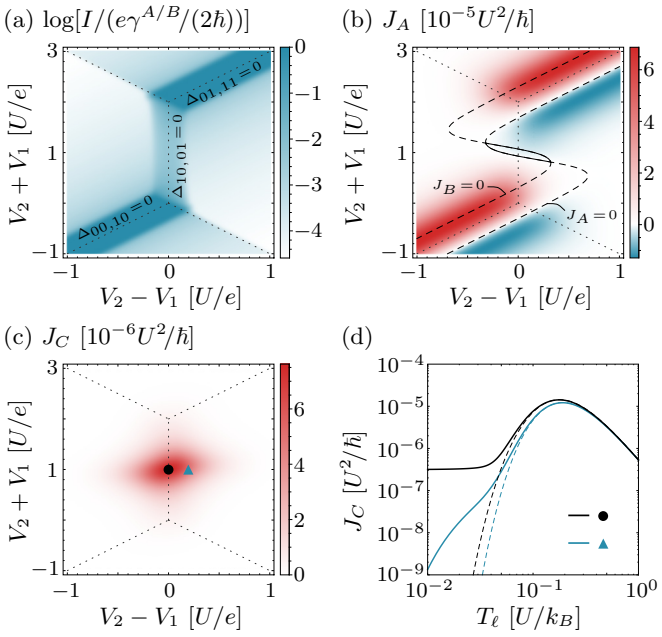

FIG. 3. Electric current and heat currents. (a) Electric current in System 1 as a function of gate detuning $V_2 - V_1$ and total gating $V_2 + V_1$ at low temperature, $k_B T_\ell = 10^{-2}\,U$. (b) Heat current in lead A, J_A, at high temperature, $k_B T_\ell = 10^{-1}\,U$ (contours indicate where J_A and J_B are zero). (c) Heat current in lead C, J_C, for $k_B T_\ell = 10^{-1}\,U$. (d) J_C as a function of temperature with (solid) and without (dashed) cotunneling for the gate configurations marked in (c): $eV_{1,2} = 0.5\,U$ (black circle) and $eV_1 = 0.4\,U$, $eV_2 = 0.6\,U$ (blue triangle). In plots (a)–(c), the degeneracy lines of the honeycomb vertex are indicated with dotted lines. Parameters: $\gamma^{A/B}(\epsilon) = 10^{-3}\,U$, $\gamma^C(\epsilon) = 10^{-2}\,U$, and $eV = 0.3\,U$.

larger magnitude outside this region). From the heat current in lead C shown in Fig. 3(c), the cooling of System 1 is seen to be at the cost of heating System 2. This Coulomb-mediated energy exchange between the two QD systems occurs in spite of the fact that no electrons are exchanged, and it is the driving force behind demon-induced cooling [9,10], energy harvesting [4,8,11,12], and Coulomb drag [26,27].

A simple analytical result for the energy exchange can be found when considering sequential tunneling processes only (indicated by the superscript s). In this case, the total heat currents in System 1, $J_1^s \equiv J_A^s + J_B^s$, and System 2, $J_2^s \equiv J_C^s$, become [11]

$$J_1^s = \frac{U}{\tau^s}(\Gamma^+ - \Gamma^-) + \frac{\mu_A - \mu_B}{e} I^s, \tag{19a}$$

$$J_2^s = \frac{U}{\tau^s}(\Gamma^- - \Gamma^+), \tag{19b}$$

where $\Gamma^- \equiv \Gamma_{00,01}\Gamma_{01,11}\Gamma_{11,10}\Gamma_{10,00}$ and $\Gamma^+ \equiv \Gamma_{00,10}\Gamma_{10,11}\Gamma_{11,01}\Gamma_{01,00}$. The factor τ^s depends on the various sequential tunneling rates, however it is merely a normalization factor and is not reproduced here. The two terms proportional to U in Eq. (19) describe the energy exchange, whereas the last term in Eq. (19a) describes the contribution from Joule heating in System 1. The direction of the energy transfer is determined by the sign of $\Gamma^- - \Gamma^+$. It is therefore convenient to consider the ratio

$$\frac{\Gamma^-}{\Gamma^+} = \Omega e^{U(\beta_2 - \beta_1)}, \tag{20}$$

which describes whether energy is transferred from System 1 to 2 ($\Gamma^-/\Gamma^+ > 1$) or vice versa ($\Gamma^-/\Gamma^+ < 1$) [48]. On the right-hand side of (20), we have taken $\beta_{A/B} = \beta_1$ and $\beta_C = \beta_2$, and have expressed the ratio in terms of an exponential factor, which depends on the temperature in System 1 and System 2, and

$$\Omega \equiv \frac{\left(\gamma_1^A f_1^A + \gamma_1^B f_1^B\right)\left(\gamma_0^A f_0^A e^{-\beta_1\mu_A} + \gamma_0^B f_0^B e^{-\beta_1\mu_B}\right)}{\left(\gamma_0^A f_0^A + \gamma_0^B f_0^B\right)\left(\gamma_1^A f_1^A e^{-\beta_1\mu_A} + \gamma_1^B f_1^B e^{-\beta_1\mu_B}\right)}, \tag{21}$$

which depends on the temperature and bias in System 1 only. The subscript 0 (1) in Eq. (21) indicates that the corresponding function is evaluated at $\Delta_{00,10}$ ($\Delta_{01,11}$) [see Eqs. (6) and (7)].

The exponential factor in (20) shows that a temperature gradient between the two QD systems can generate a net heat flow from the hot to the cold system. This is the mechanism behind the heat engine studied in Ref. [11]. On the other hand, a closer inspection of the Ω factor reveals that it is, in fact, possible to generate a net heat flow in the opposite direction, i.e., from the cold to the hot system, and this is the cause of the negative heat current at the center of Fig. 3(b). This so-called demon-induced cooling effect will be discussed further in Sec. V B below.

When the applied bias and temperature are small compared to the interdot Coulomb interaction, $eV, k_B T \ll U$, cotunneling processes start to dominate the heat currents in the center of the stability diagram. This is demonstrated in Fig. 3(d), which shows the heat current J_C as a function of temperature for the two different gate tunings marked with symbols in Fig. 3(c). Considering sequential tunneling only (dashed curves), the heat current is quenched at $k_B T \ll U$ as $\Gamma_{01,11}$ and $\Gamma_{10,00}$ in Γ^- become exponentially suppressed. This can also be understood from the illustration in Fig. 4(a), which shows the sequence of

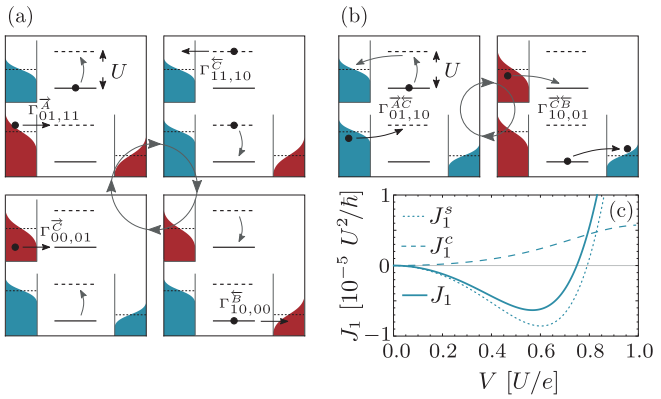

FIG. 4. Cooling cycle and effect of cotunneling. (a) Sequence of sequential tunneling processes that cool System 1. The positions of the dot levels when the other dot is empty (occupied) is illustrated with solid (dotted) lines. (b) Sequence of nonlocal cotunneling processes. (c) Heat current J_1 as a function of bias voltage. The individual contributions from sequential (J_1^s) and cotunneling (J_1^c) are also shown. Parameters: $eV_1 = eV_2 = U/2$, $\gamma^{A/B}(\epsilon) = 10^{-3}\,U$, $\gamma^C(\epsilon) = 10^{-2}\,U$, and $k_B T = 0.1\,U$.

sequential tunneling processes corresponding to Γ^-. However, nonlocal cotunneling processes allow the system to fluctuate between the two states $10 \leftrightarrow 01$, as illustrated in Fig. 4(b), and thereby transfer heat between the systems. The nonlocal cotunneling channel is open for $|\Delta_{01,10}| \lesssim \max\{|eV/2|, k_BT\}$, and the associated heat current is thus also suppressed at low temperature when $\Delta_{01,10} \neq 0$, as illustrated by the blue curve (triangle) in Fig. 3(d). For zero detuning, $\Delta_{01,10} = 0$ (circle), the nonlocal cotunneling rates, and hence also the heat current, saturate at $k_BT \ll eV$. In Sec. V B, we demonstrate that nonlocal cotunneling processes have a significant effect on the demon-induced cooling mechanism.

B. Demon-induced cooling

The effect of cooling System 1 at the cost of heating System 2 has recently been discussed in the context of a Maxwell's demon, where System 2 plays the role of the demon that performs the necessary feedback to cool System 1 [9,10]. To maximize the achievable cooling power for refrigeration purposes [49], large tunneling rates, $\gamma^\ell(\epsilon) \sim k_BT, U$, are desirable [cf. Eq. (19)]. However, large tunneling rates increase the contribution from higher-order tunneling processes, thus emphasizing the importance of including cotunneling processes in the analysis.

In the following, we consider the case of uniform temperature $T_\ell \equiv T$ whereby the exponential factor in (20) becomes unity. This allows us to focus on the Ω factor in the optimization of the performance. Equation (19) shows that the cooling mechanism is governed by Γ^- since, as illustrated in Fig. 4(a), in a full sequential cycle an amount of energy U is transferred from System 1 to System 2, thereby cooling System 1. In the following, we discuss how to increase the cooling power by maximizing the success rate for completing the cooling cycle in Fig. 4(a).

1. Cotunneling limitations

Although the cycle of nonlocal cotunneling processes illustrated in Fig. 4(b) gives the same net transfer of electrons as the sequential tunneling cycle in Fig. 4(a), the net energy transfer is different for the two cases. As illustrated, in a cotunneling process also electrons below (above) the electrochemical potential can tunnel out of lead A (into lead B), and thus reduce the demon-induced cooling effect.

In Fig. 4(c), we show the heat current $J_1 = J_A + J_B$ together with its individual contributions from sequential (J_1^s) and cotunneling (J_1^c) processes. Overall, System 1 cools at low bias, while at higher bias, Joule heating becomes dominant. The minimum in J_1 as a function of bias voltage is referred to as the maximum cooling power, $J_{1,\max} \equiv \min J_1(V)$. As the figure shows, cotunneling reduces the maximum cooling power.

Figure 5 shows how the maximum cooling power $J_{1,\max}$ scales with the lead coupling strengths. As the figure demonstrates, the rates must satisfy $\gamma^C > \gamma^{A/B}$ to ensure that System 2 acts sufficiently fast to perform the desired feedback such that the cooling cycle in Fig. 4(a) is completed when an electron tunnels between leads A and B [49]. In the region of large cooling power, cotunneling processes start to become important, and hence there is a tradeoff between sequential tunneling, which improves the cooling effect, and nonlocal cotunneling, which limits the effect. In addition, the area in the lead coupling parameter space where refrigeration is possible is also reduced when cotunneling is included.

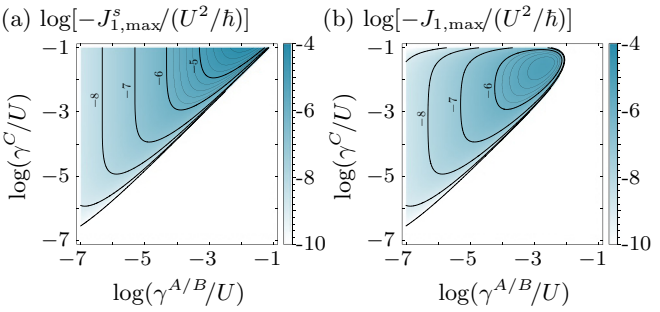

FIG. 5. Maximum cooling power, $J_{1,\max}$, as a function of the lead coupling strengths for energy-independent couplings. (a) Sequential tunneling and (b) sequential plus cotunneling. Parameters: $eV_1 = eV_2 = U/2$ and $k_BT = 0.1\,U$.

2. Performance boosting

Here we demonstrate that energy-dependent lead couplings can enhance the demon-induced cooling power significantly. We restrict the discussion to lead couplings with a linear energy dependence [cf. Eq. (18)].

By inspecting the Ω factor in Eq. (21), we find that for $\mu_A > \mu_B$, the configuration illustrated in the inset of Fig. 6, where γ_0^A, γ_1^B are reduced compared to γ_1^A, γ_0^B, boosts the Ω factor (and thereby Γ^-/Γ^+). This results in an enhancement of the cooling power by suppressing tunneling between leads A and B via two sequential tunneling processes, while at the

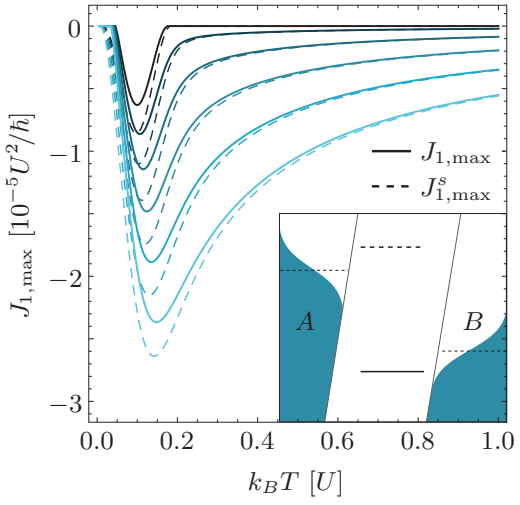

FIG. 6. Performance boosting with energy-dependent lead couplings. Maximum cooling power as function of temperature for different lead coupling strengths: $\partial\gamma^A = -\partial\gamma^B = x\gamma_0^{A/B}/U$ (sketched in the inset), with $x = 0$ (black) to $x = 1$ (light blue) in steps of 0.2. The full (dashed) lines show the result obtained with (without) cotunneling. Parameters: $\gamma^C(\epsilon) = 10^{-2}\,U$, $\gamma_0^{A/B} = 10^{-3}\,U$, $eV_1 = eV_2 = U/2$, and $\eta = 10^{-4}\,U$.

same time promoting the processes of the cooling cycle in Fig. 4(a).

In Fig. 6 we show the maximum cooling power as a function of temperature for different situations for the energy dependence of the lead couplings, from the top (black) curve showing the result for energy-*independent* lead couplings, to increasing energy dependence, i.e., increasing $|\partial\gamma^{A/B}|$, toward the bottom (light blue) curve. When tuning the energy dependence of the lead couplings, a significant enhancement of the cooling power is achieved. Again, the effect of cotunneling processes is to reduce the attainable cooling power (solid lines) relative to the cooling power obtained when only considering sequential tunneling processes (dashed lines).

VI. CONCLUSIONS

In summary, we have studied thermoelectric effects in CCQD systems with a T-matrix based master-equation approach for the calculation of charge and heat currents. The method (i) treats *incoherent* sequential tunneling processes and *coherent* cotunneling processes on an equal footing, and (ii) can account for energy-dependent tunnel couplings to the leads. Both are important for quantitative predictions and optimization of the thermoelectric properties of CCQDs.

To benchmark the master-equation method, we considered a noninteracting single-level QD coupled to source and drain leads for which the Landauer-Büttiker formalism is exact. In the regime of validity of our method, i.e., small tunnel couplings to the leads, $\gamma < k_B T$, we demonstrated excellent agreement with the results from the Landauer-Büttiker method when cotunneling processes are included in the master equation.

Furthermore, we studied the effect of cotunneling processes and energy-dependent lead couplings on the thermoelectric properties of a CCQD system consisting of two QDs exhibiting a Maxwell's-demon-like cooling mechanism [9,10]. First of all, we showed that cotunneling processes reduce the cooling effect since they do not share the delicate energy selectivity inherent to sequential tunneling processes. This results in a significant reduction of the achievable cooling power compared to the sequential tunneling result when the lead couplings are increased to maximize the cooling power from sequential tunneling processes. Secondly, we demonstrated that it is possible to boost the cooling power significantly via other means by introducing energy-dependent lead couplings and properly tuning their energy dependence. In this case, we showed that cotunneling still reduces the cooling power significantly, thus emphasizing the importance of cotunneling processes in quantitative analyses.

Applying the methodology to other mesoscopic systems allows for testing of new thermoelectric device ideas beyond sequential tunneling estimates, as well as for improved comparison with experiments.

ACKNOWLEDGMENTS

We would like to thank J. P. Pekola, M. Leijnse, C. Timm, and N. M. Gergs for valuable discussions. K.K. acknowledges support from the European Union's Horizon 2020 research and innovation programme under the Marie Sklodowska–Curie Grant Agreement No. 713683 (COFUNDfellowsDTU). The Center for Nanostructured Graphene (CNG) is sponsored by the Danish Research Foundation, Project DNRF103.

APPENDIX: COTUNNELING RATES AND REGULARIZATION PROCEDURE

The rate for elastic cotunneling through a single-level QD is given by

$$\tilde{\Gamma}^{\vec{\ell}\,\overleftarrow{\ell'}}_{mm} = \int \frac{d\epsilon}{2\pi\hbar}\gamma^{\ell}(\epsilon)\gamma^{\ell'}(\epsilon) f^{\ell}(\epsilon)\bar{f}^{\ell'}(\epsilon)\left|\frac{1}{\Delta_{vm}\pm\epsilon+i\eta}\right|^2, \tag{A1}$$

where v refers to the virtually occupied intermediate state created in the process in which an initially empty level is filled ($+\epsilon$) or an initially filled level is emptied ($-\epsilon$).

In pair-cotunneling processes, two electrons tunnel simultaneously out of (into) the QD system and into (out of) the leads ℓ and ℓ'. The rate for such processes takes the form

$$\tilde{\Gamma}^{\overleftarrow{\ell}\,\overleftarrow{\ell'}}_{mn} = \int \frac{d\epsilon}{2\pi\hbar}\gamma^{\ell}(\epsilon)\gamma^{\ell'}(\Delta_{nm}-\epsilon)\bar{f}^{\ell}(\epsilon)\bar{f}^{\ell'}(\Delta_{nm}-\epsilon) \times\left|\frac{1}{\Delta_{vm}-\epsilon+i\eta}+\frac{1}{\Delta_{v'n}+\epsilon+i\eta}\right|^2, \tag{A2}$$

where v (v') refers to the virtually occupied intermediate state in a process in which an electron initially tunnels from the QD system and into lead ℓ (ℓ'). Similarly,

$$\tilde{\Gamma}^{\vec{\ell}\,\vec{\ell'}}_{mn} = \int \frac{d\epsilon}{2\pi\hbar}\gamma^{\ell}(\epsilon)\gamma^{\ell'}(\Delta_{mn}-\epsilon) f^{\ell}(\epsilon) f^{\ell'}(\Delta_{mn}-\epsilon) \times\left|\frac{1}{\Delta_{vn}-\epsilon+i\eta}+\frac{1}{\Delta_{v'm}+\epsilon+i\eta}\right|^2, \tag{A3}$$

where v (v') refers to the virtually occupied intermediate state in a process in which an electron initially tunnels from lead ℓ' (ℓ) and into the QD system.

The bare cotunneling rates are formally divergent in the limit $\eta \to 0$. The divergence stems from factors involving $|x+i\eta|^{-2}$, $x,\eta \in \mathbb{R}$. Using the fact that [29]

$$\left|\frac{1}{x+i\eta}\right|^2 \to \frac{\pi}{\eta}\delta(x)+\mathcal{P}\frac{1}{x^2}, \quad \eta\to 0^+, \tag{A4}$$

where $\mathcal{P}$ denotes the principal value, we can identify the divergent contributions, e.g., from Eq. (8),

$$\tilde{\Gamma}^{\vec{\ell}\,\overleftarrow{\ell'}}_{mn} \to \frac{\hbar}{2\eta}\left(\Gamma^{\vec{\ell}}_{mv}\Gamma^{\overleftarrow{\ell'}}_{vn}+\Gamma^{\overleftarrow{\ell'}}_{mv'}\Gamma^{\vec{\ell}}_{v'n}\right)+\Gamma^{\vec{\ell}\,\overleftarrow{\ell'}}_{mn}, \tag{A5}$$

where $\Gamma^{\vec{\ell}\,\overleftarrow{\ell'}}_{mn}$ denotes the regularized cotunneling rate, and we have used the fact that the cross-terms from the absolute squared in Eq. (8) do not contribute to any divergences. The divergent contribution is proportional to products of two sequential tunneling rates. These correspond to two energy-conserving (sequential) transitions that can be identified with the intermediate processes in the cotunneling process. The sum is over the possible sequences of intermediate transitions. Similarly, for the cotunneling heat rates, e.g., Eq. (12),

$$\tilde{W}^{\vec{\ell}\,\overleftarrow{\ell'}}_{\ell,mn} \to \frac{\hbar}{2\eta}\left[W^{\vec{\ell}}_{\ell,mv}\Gamma^{\overleftarrow{\ell'}}_{vn}+\Gamma^{\overleftarrow{\ell'}}_{mv'}W^{\vec{\ell}}_{\ell,v'n}\right]+W^{\vec{\ell}\,\overleftarrow{\ell'}}_{\ell,mn}, \tag{A6}$$

or the corresponding heat rate in lead ℓ',

$$\tilde{W}^{\vec{\ell}\,\vec{\ell'}}_{\ell',mn} \to \frac{\hbar}{2\eta}\left[\Gamma^{\vec{\ell}}_{mv} W^{\vec{\ell'}}_{\ell',vn} + W^{\vec{\ell'}}_{\ell',mv'}\Gamma^{\vec{\ell}}_{v'n}\right] + W^{\vec{\ell}\,\vec{\ell'}}_{\ell',mn}. \tag{A7}$$

We apply the regularization scheme in Ref. [29] and subtract the terms scaling as η^{-1}.

In the case of identical temperatures in the leads, using the identity $f(\epsilon_1)[1-f(\epsilon_2)] = n(\epsilon_1-\epsilon_2)[f(\epsilon_2)-f(\epsilon_1)]$, where $f(\epsilon)$ is the Fermi-Dirac distribution and $n(\epsilon)$ is the Bose-Einstein distribution, the cotunneling rates can be written in the form

$$I = \int_{-\infty}^{\infty} d\epsilon\, P(\epsilon)[f^{\ell'}(\epsilon) - f^{\ell}(\epsilon+\Delta_3)] \times \left|\frac{k_1}{\epsilon-\Delta_1+i\eta} + \frac{k_2}{\Delta_2-\epsilon+i\eta}\right|^2, \tag{A8}$$

where $P(\epsilon)$ is assumed to be a polynomial, $P(\epsilon) = \sum_{i=0}^{n} c_i \epsilon^n$, of maximum order $n=2$ for $k_1 - k_2 \neq 0$ and $n=4$ for $k_1 - k_2 = 0$ to ensure that the result below is well-defined. The derivation is in line with the one in Ref. [27], and the integral becomes

$$\begin{aligned} I = {} & k_1^2 P'(\Delta_1)\mathrm{Re}[\psi^-_{\ell'}(\Delta_1) - \psi^-_{\ell}(\Delta_1+\Delta_3)] + \frac{k_1^2\beta}{2\pi}P(\Delta_1)\mathrm{Im}[\psi^-_{1_{\ell'}}(\Delta_1) - \psi^-_{1_{\ell}}(\Delta_1+\Delta_3)] \\ & + k_2^2 P'(\Delta_2)\mathrm{Re}[\psi^-_{\ell'}(\Delta_2) - \psi^-_{\ell}(\Delta_2+\Delta_3)] + \frac{k_2^2\beta}{2\pi}P(\Delta_2)\mathrm{Im}[\psi^-_{1_{\ell'}}(\Delta_2) - \psi^-_{1_{\ell}}(\Delta_2+\Delta_3)] \\ & - \frac{2k_1k_2}{\Delta_1-\Delta_2}(P(\Delta_1)\mathrm{Re}[\psi^-_{\ell'}(\Delta_1) - \psi^-_{\ell}(\Delta_1+\Delta_3)] - P(\Delta_2)\mathrm{Re}[\psi^-_{\ell'}(\Delta_2) - \psi^-_{\ell}(\Delta_2+\Delta_3)]) + R + O(\eta^{-1}) + O(\eta), \end{aligned} \tag{A9}$$

where

$$\psi^{\pm}_{(1)_\ell}(\epsilon) \equiv \psi_{(1)}\left(\frac{1}{2} \pm i\frac{\beta}{2\pi}(\epsilon-\mu_\ell)\right), \tag{A10}$$

with ψ (ψ_1) being the digamma (trigamma) function, and

$$R = \begin{cases} c_2(\mu_{\ell'} - \mu_\ell + \Delta_3)(k_1-k_2)^2, & k_1 - k_2 \neq 0, \\ c_4(\mu_{\ell'} - \mu_\ell + \Delta_3)k_1^2(\Delta_1-\Delta_2)^2, & k_1 - k_2 = 0. \end{cases} \tag{A11}$$

The term $O(\eta^{-1})$ is omitted by regularization before taking the limit $\eta \to 0$. For $k_BT < \gamma$ (outside the regime of validity), the failure of the approach is seen as a logarithmic divergence of the digamma functions near the degeneracy points.

In studies of thermoelectric effects where different lead temperatures as well as more general energy dependence of the lead couplings become relevant, one must turn to a numerical procedure. In this case, we evaluate the cotunneling integrals numerically with a small but finite η, and subsequently subtract contributions of order η^{-1} as shown in, e.g., Eqs. (A5)–(A7). In particular, we have applied the numerical procedure in Figs. 2 and 6, and we have stated the values of η in the figure captions.

[1] J. P. Pekola, O.-P. Saira, V. F. Maisi, A. Kemppinen, M. Möttönen, Y. A. Pashkin, and D. V. Averin, Single-electron current sources: Toward a refined definition of the ampere, Rev. Mod. Phys. **85**, 1421 (2013).

[2] F. Giazotto, T. T. Heikkilä, A. Luukanen, A. M. Savin, and J. P. Pekola, Opportunities for mesoscopics in thermometry and refrigeration: Physics and applications, Rev. Mod. Phys. **78**, 217 (2006).

[3] M. S. Dresselhaus, G. Chen, M. Y. Tang, R. G. Yang, H. Lee, D. Z. Wang, Z. F. Ren, J.-P. Fleurial, and P. Gogna, New directions for low-dimensional thermoelectric materials, Adv. Mater. **19**, 1043 (2007).

[4] H. Thierschmann, R. Sánchez, B. Sothmann, H. Buhmann, and L. W. Molenkamp, Thermoelectrics with Coulomb-coupled quantum dots, C. R. Phys. **17**, 1109 (2016).

[5] D. Bischoff, M. Eich, O. Zilberberg, C. Rössler, T. Ihn, and K. Ensslin, Measurement back-action in stacked graphene quantum dots, Nano. Lett. **15**, 6003 (2015).

[6] A. J. Keller, J. S Lim, D. Sánchez, R. López, S. Amasha, J. A. Katine, H. Shtrikman, and D. Goldhaber-Gordon, Cotunneling Drag Effect in Coulomb-Coupled Quantum Dots, Phys. Rev. Lett. **117**, 066602 (2016).

[7] A. Hamo, A. Benyamini, I. Shapir, I. Khivrich, J. Waissman, K. Kaasbjerg, Y. Oreg, F. von Oppen, and S. Ilani, Electron attraction mediated by Coulomb repulsion, Nature (London) **535**, 395 (2016).

[8] H. Thierschmann, R. Sánchez, B. Sothmann, F. Arnold, C. Heyn, W. Hansen, H. Buhmann, and L. W. Molenkamp, Three-terminal energy harvester with coupled quantum dots, Nat. Nanotech. **10**, 854 (2015).

[9] J. V. Koski, A. Kutvonen, I. M. Khaymovich, T. Ala-Nissila, and J. P. Pekola, On-Chip Maxwell's Demon as an Information-Powered Refrigerator, Phys. Rev. Lett. **115**, 260602 (2015).

[10] P. Strasberg, G. Schaller, T. Brandes, and M. Esposito, Thermodynamics of a Physical Model Implementing a Maxwell Demon, Phys. Rev. Lett. **110**, 040601 (2013).

[11] R. Sánchez and M. Büttiker, Optimal energy quanta to current conversion, Phys. Rev. B **83**, 085428 (2011).

[12] B. Sothmann, R. Sánchez, and A. N. Jordan, Thermoelectric energy harvesting with quantum dots, Nanotechnology **26**, 032001 (2014).

[13] R. Sánchez, H. Thierschmann, and L. W. Molenkamp, All-thermal transistor based on stochastic switching, Phys. Rev. B **95**, 241401(R) (2017).

[14] J. V. Koski and J. P. Pekola, Maxwell's demons realized in electronic circuits, C. R. Phys. **17**, 1130 (2016).

[15] G. Benenti, G. Casati, K. Saito, and R. S. Whitney, Fundamental aspects of steady-state conversion of heat to work at the nanoscale, Phys. Rep. **694**, 1 (2017).

[16] F. Haupt, M. Leijnse, H. L. Calvo, L. Classen, J. Splettstoesser, and M. R. Wegewijs, Heat, molecular vibrations, and adiabatic driving in non-equilibrium transport through interacting quantum dots, Phys. Status Solidi B **250**, 2315 (2013).

[17] M. Leijnse, M. R. Wegewijs, and K. Flensberg, Nonlinear thermoelectric properties of molecular junctions with vibrational coupling, Phys. Rev. B **82**, 045412 (2010).

[18] J. Argüello-Luengo, D. Sánchez, and R. López, Heat asymmetries in nanoscale conductors: The role of decoherence and inelasticity, Phys. Rev. B **91**, 165431 (2015).

[19] D. Sánchez and R. López, Nonlinear phenomena in quantum thermoelectrics and heat, C. R. Phys. **17**, 1060 (2016).

[20] N. M. Gergs, C. B. M. Hörig, M. R. Wegewijs, and D. Schuricht, Charge fluctuations in nonlinear heat transport, Phys. Rev. B **91**, 201107(R) (2015).

[21] K. M. Seja, G. Kiršanskas, C. Timm, and A. Wacker, Violation of Onsager's theorem in approximate master equation approaches, Phys. Rev. B **94**, 165435 (2016).

[22] A.-M. Daré and P. Lombardo, Powerful Coulomb-drag thermoelectric engine, Phys. Rev. B **96**, 115414 (2017).

[23] H. Bruus and K. Flensberg, *Many-body Quantum Theory in Condensed Matter Physics* (Oxford University Press, Oxford, 2004).

[24] J. Waissman, M. Honig, S. Pecker, A. Benyamini, A. Hamo, and S. Ilani, Realization of pristine and locally tunable one-dimensional electron systems in carbon nanotubes, Nat. Nanotech. **8**, 569 (2013).

[25] Y. Zhang, G. Lin, and J. Chen, Three-terminal quantum-dot refrigerators, Phys. Rev. E **91**, 052118 (2015).

[26] R. Sánchez, R. López, D. Sánchez, and M. Büttiker, Mesoscopic Coulomb Drag, Broken Detailed Balance, and Fluctuation Relations, Phys. Rev. Lett. **104**, 076801 (2010).

[27] K. Kaasbjerg and A.-P. Jauho, Correlated Coulomb Drag in Capacitively Coupled Quantum-Dot Structures, Phys. Rev. Lett. **116**, 196801 (2016).

[28] J. S. Lim, R. Löpez, and D. Sánchez, Engineering drag currents in Coulomb coupled quantum dots, arXiv:1612.06627 (2016).

[29] M. Turek and K. A. Matveev, Cotunneling thermopower of single electron transistors, Phys. Rev. B **65**, 115332 (2002).

[30] J. Koch, F. von Oppen, Y. Oreg, and E. Sela, Thermopower of single-molecule devices, Phys. Rev. B **70**, 195107 (2004).

[31] C. Timm, Tunneling through molecules and quantum dots: Master-equation approaches, Phys. Rev. B **77**, 195416 (2008).

[32] J. König, J. Schmid, H. Schoeller, and G. Schön, Resonant tunneling through ultrasmall quantum dots: Zero-bias anomalies, magnetic-field dependence, and boson-assisted transport, Phys. Rev. B **54**, 16820 (1996).

[33] A. Thielmann, M. H. Hettler, J. König, and G. Schön, Cotunneling Current and Shot Noise in Quantum Dots, Phys. Rev. Lett. **95**, 146806 (2005).

[34] J. N. Pedersen and A. Wacker, Tunneling through nanosystems: Combining broadening with many-particle states, Phys. Rev. B **72**, 195330 (2005).

[35] C. Timm, Time-convolutionless master equation for quantum dots: Perturbative expansion to arbitrary order, Phys. Rev. B **83**, 115416 (2011).

[36] S. Amasha, A. J. Keller, I. G. Rau, A. Carmi, J. A. Katine, H. Shtrikman, Y. Oreg, and D. Goldhaber-Gordon, Pseudospin-Resolved Transport Spectroscopy of the Kondo Effect in a Double Quantum Dot, Phys. Rev. Lett. **110**, 046604 (2013).

[37] J. Koch, M. E. Raikh, and F. von Oppen, Pair Tunneling Through Single Molecules, Phys. Rev. Lett. **96**, 056803 (2006).

[38] M. Leijnse, M. R. Wegewijs, and M. H. Hettler, Pair Tunneling Resonance in the Single-Electron Transport Regime, Phys. Rev. Lett. **103**, 156803 (2009).

[39] S. Koller, M. Grifoni, M. Leijnse, and M. R. Wegewijs, Density-operator approaches to transport through interacting quantum dots: Simplifications in fourth order perturbation theory, Phys. Rev. B **82**, 235307 (2010).

[40] Notice that for the particular pair-cotunneling processes with $\ell = \ell'$, one should include a factor of 2 in the current; however, for single-level QDs discussed here, such processes do not contribute.

[41] M. F. Ludovico, M. Moskalets, D. Sánchez, and L. Arrachea, Dynamics of energy transport and entropy production in ac-driven quantum electron systems, Phys. Rev. B **94**, 035436 (2016).

[42] J. Koch, F. von Oppen, and A. V. Andreev, Theory of the Franck-Condon blockade regime, Phys. Rev. B **74**, 205438 (2006).

[43] H. Haug and A.-P. Jauho, *Quantum Kinetics in Transport and Optics of Semiconductors* (Springer, Berlin, 2008).

[44] A. V. Feshchenko, J. V. Koski, and J. P. Pekola, Experimental realization of a Coulomb blockade refrigerator, Phys. Rev. B **90**, 201407 (2014).

[45] W. Lee, K. Kim, W. Jeong, L. A. Zotti, F. Pauly, J. C. Cuevas, and P. Reddy, Heat dissipation in atomic-scale junctions, Nature (London) **498**, 209 (2013).

[46] In the numerical calculations we take the absolute value of the lead coupling strengths to ensure that the linear expansion yields non-negative coupling strengths.

[47] W. G. van der Wiel, S. De Franceschi, J. M. Elzerman, T. Fujisawa, S. Tarucha, and L. P. Kouwenhoven, Electron transport through double quantum dots, Rev. Mod. Phys. **75**, 1 (2002).

[48] R. Sánchez and M. Büttiker, Detection of single-electron heat transfer statistics, Europhys. Lett. **100**, 47008 (2012).

[49] A. Kutvonen, J. Koski, and T. Ala-Nissila, Thermodynamics and efficiency of an autonomous on-chip Maxwell's demon, Sci. Rep. **6**, 21126 (2016).